Developmental Cell
Article

Protein Aggregation Behavior Regulates Cyclin Transcript Localization and Cell-Cycle Control

ChangHwan Lee,[1] Huaiying Zhang,[1] Amy E. Baker,[1] Patricia Occhipinti,[1] Mark E. Borsuk,[2] and Amy S. Gladfelter[1,*]
[1]Department of Biological Sciences
[2]Thayer School of Engineering
Dartmouth College, Hanover, NH 03755, USA
*Correspondence: amy.gladfelter@dartmouth.edu
http://dx.doi.org/10.1016/j.devcel.2013.05.007

SUMMARY

Little is known about the active positioning of transcripts outside of embryogenesis or highly polarized cells. We show here that a specific G1 cyclin transcript is highly clustered in the cytoplasm of large multinucleate cells. This heterogeneous cyclin transcript localization results from aggregation of an RNA-binding protein, and deletion of a polyglutamine stretch in this protein results in random transcript localization. These multinucleate cells are remarkable in that nuclei cycle asynchronously despite sharing a common cytoplasm. Notably, randomization of cyclin transcript localization significantly diminishes nucleus-to-nucleus differences in the number of mRNAs and synchronizes cell-cycle timing. Thus, nonrandom cyclin transcript localization is important for cell-cycle timing control and arises due to polyQ-dependent behavior of an RNA-binding protein. There is a widespread association between polyQ expansions and RNA-binding motifs, suggesting that this is a broadly exploited mechanism to produce spatially variable transcripts and heterogeneous cell behaviors.

INTRODUCTION

Regulated positioning of mRNAs has long been appreciated within the large cytoplasm of eggs where gradients of maternally deposited transcripts give rise to body plan patterns such as the anterior-posterior axis in *Drosophila* development (Berleth et al., 1988; Weil et al., 2006). Similarly, there are known roles for transcript transport and localized translation in highly polarized cells such as neurons and even in budding yeast (Takizawa et al., 2000; van den Bogaart et al., 2009; Wu et al., 2007). However, there is little known about the active positioning of transcripts outside of embryogenesis or highly polarized cells. Cytoplasmic granules including P-bodies and stress granules are one general way mRNAs can be gathered in a specific location in the cytoplasm or near nuclei (Decker and Parker, 2012). In vivo, these RNA granules are thought to be sites of mRNA degradation, localized translation, or the means by which transcripts can be collectively transported in the cell. However, the dynamic assembly and disassembly of such large RNA clusters are not well understood. Additionally, there is evidence of smaller scale positioning of transcripts independent of large granules like P-bodies. For example, dozens of different patterns of mRNA localization have been reported in global studies of transcripts in *Drosophila* embryos yet the mechanisms underlying these patterns remain largely unknown (Lécuyer et al., 2007). Control of mRNA localization is still a frontier of posttranscriptional regulation and a key aspect of understanding the organization of the cytoplasm (Lécuyer et al., 2009).

Recent work suggests that unstructured regions of RNA-binding proteins have the capacity in vitro to form biogels that mimic cellular RNA granules (Han et al., 2012; Kato et al., 2012). There is a high association between RNA-binding domains and low complexity structure or polyQ expansions. This suggests that protein aggregation could play a physiological role in generally positioning transcripts not only through RNA granules but also potentially in smaller scale assemblies that contribute to organization of the cytoplasm (King et al., 2012). Evidence from work on yeast prions points to possible physiological roles for polyQ domains in adaptability, and work in *Aplysia* and *Drosophila* neurons has indicated that prion-like behavior regulates translation of transcripts implicated in the formation of long-term memory (Halfmann et al., 2012a; Majumdar et al., 2012; Si et al., 2003). After decades of focus on the pathological roles of assemblies of unstructured proteins, there are hints of useful roles for protein aggregates in cell physiology and organization. Here, we link aggregation behavior of an RNA-binding protein to cell-cycle control through the nonrandom positioning of cyclin transcripts.

Cell-cycle transitions in eukaryotes are driven by the periodic accumulation and destruction of cyclins. Diffusible cyclin/cyclin-dependent kinase (CDK) complexes synchronize the behavior of nuclei artificially induced to share the same cytoplasm via cell-cell fusion or in cell-free cycling extracts (Johnson and Rao, 1970, 1971). The multinucleate fungus *Ashbya gossypii* presents a major challenge to these current cell-cycle-control paradigms. In this and other multinucleate cells, neighboring nuclei are at different stages of the cell cycle (Cardoso et al., 1993; Gladfelter, 2006; Gladfelter et al., 2006). Asynchronous nuclear division in a common cytoplasm requires that nuclei cycle autonomously. The mechanisms underlying such autonomous behavior remain mysterious.

A. gossypii is closely related to *Saccharomyces cerevisiae*, and, as in *S. cerevisiae*, transcriptionally-regulated G1 cyclins control the G1/S transition (Dietrich et al., 2004; Nair et al.,

2010). However, despite sharing a common cytoplasm, neighboring nuclei in *A. gossypii* differ widely in the timing of cell-cycle events, implying that the transcriptional output of one nucleus does not equally affect all local nuclei (Gladfelter et al., 2006). Asynchrony of nuclei in a shared cytoplasm is promoted by a widely conserved G1/S transcriptional regulatory circuit that controls G1 cyclin synthesis, raising an apparent conundrum: how can transcription factors promote cycle timing differences between neighboring nuclei given that the transcripts produced by one nucleus must exit their nuclear birthplace and commingle in the common cytosol? A potential resolution of the conundrum would be that transcripts are not, in fact, shared equally by all nuclei, so that individual nuclei can establish differentiated islands of cytoplasm that promote asynchronous cycling. Such domains of cytoplasm may be similar to the energids that form around nuclei in the *Drosophila* syncytial embryo. These may be compartmentalized by endomembrane, as has been seen in *Drosophila*, or by some other cytoplasmic organization that may restrict diffusion between nuclei (Mavrakis et al., 2009a, 2009b). Here, we demonstrate that *CLN3* transcripts are clustered due to an RNA-binding protein called Whi3 that was previously shown to potentially regulate Cln3 translation in *S. cerevisiae* (Garí et al., 2001; Nash et al., 2001; Wang et al., 2004). *Ashbya* Whi3 has a notable expansion of glutamines that causes Whi3 protein aggregation in the cytoplasm and therefore promotes heterogeneous cyclin transcript distribution and asynchronous nuclear cycling. This study reveals a normal physiological role for polyQ expansions that are conventionally considered primarily in pathological contexts and links them both to transcript localization and cell-cycle control.

RESULTS

The G1 Cyclin *CLN3* Transcript Shows Nonrandom Spatial Clustering

We hypothesized that spatially heterogeneous cyclin transcript abundance generates asynchronous nuclear division cycles in multinucleate *Ashbya* cells. We used single-molecule RNA fluorescence in situ hybridization (FISH) to localize transcripts encoding two different G1 cyclins (Cln1/2 and Cln3), two B-type cyclins (Clb1/2 and Clb5/6), and a glycolysis protein (Gpm2/3, presumed to be independent of the cell cycle) in *Ashbya* cells (Zenklusen and Singer, 2010). In this approach 30–48 short oligomers, each with a fluorescent probe, were synthesized with homology to the coding sequence of each transcript and applied to wild-type *Ashbya* cells. *CLN3*, *CLB1/2*, *CLB5/6*, and *GPM2/3* transcripts could be found throughout the cell without preference to sites of growth whereas *CLN1/2* transcript was highly polarized in addition to being found throughout the cytosol (Figure 1). No signal was detected in null mutants, indicating that the probes were specific to the transcripts of interest (Figures 1C and 1D).

To quantify the transcript abundance and spatial distribution, MATLAB code was written to identify the 3D coordinates of each mRNA spot in the cell, the intensity of the spot, the center of each nucleus, and the cell boundaries. Coordinates were determined for hundreds of points in tens of cells (55–170) for each transcript to analyze the density and spatial patterns of mRNA localization in an objective and automated manner (Figure 1H; Figure S1 available online). The majority of the cytosolic spots were of the same intensity, indicating that they likely represent single molecules (Figures 2A and S2). We then measured the nearest neighbor distances between transcripts to begin to assess their spatial distribution. Interestingly, although most transcripts show a normal distribution of nearest neighbor intertranscript distances (Figure S2), *CLN3* shows a striking bimodal distribution, suggesting that these transcripts are clustered in the cytoplasm (Figure 2B).

To further assess whether there is any structural pattern or clustering to the localization of cyclin transcripts in the cytosol, we used a method of spatial point pattern analysis called Ripley's K function (Kiskowski et al., 2009; Ripley, 1977). Ripley's K is based on the ratio of the number of mRNA points within a distance d of each mRNA point to the overall mRNA density of the cell (Figure 2C). The function K(d) calculated from data is then tested against the null hypothesis of complete spatial randomness (CSR) to identify any clustering in transcript positioning. Conditions of CSR were represented using 100 simulations of random (Poisson-distributed) mRNA locations for each observed cell, with mRNA density, cell geometry, and nuclear position matching those recorded for the cell (Figure 1H, bottom). These random sets were used to create 95% confidence bounds on K(d) expected to result from CSR (Figure 2C, middle panel, dotted lines). Statistically significant clustering (or dispersion) in observed cells can then be identified graphically as breaching of these bounds by empirical K(d) functions from the data images (Figure 2C). Transformation and normalization of observed and simulated K(d) functions was performed to account for differing transcript density, cell geometry, and nuclear spacing across the many observed cells, as described in Experimental Procedures (Figure 2C, bottom panel). Transformed and normalized functions are referred to as H(d)* in experimental procedures and "Clustering Index" on the plots. Clustering index values >1.0 indicate points that are significantly more clustered than random, and values <−1.0 indicate points that are significantly more dispersed than random (Figures 2C and S3).

From the resulting plots (Figures 2D and 2E), it is clear that *CLN3* mRNAs are not spatially random and appear to be highly clustered in the cytoplasm with a high and statistically significant clustering index. In contrast, the other cyclin transcripts and the glycolytic factor *GPM2/3* are generally consistent with the hypothesis of spatially random, with clustering values that rarely extend beyond the statistically significant values of ±1.0 (Figures 2D and 2E). Interestingly, in the cytosol >10 μm from hyphal tips, the *CLN1/2* transcripts appear to be dispersed (values <−1.0) rather than either clustered or completely random. Thus, only *CLN3*, and not other cyclin transcripts or the glycolytic factor GPM2/3, shows spatially nonrandom clustering in the cytoplasm.

Disruption of the Whi3-RRM-CLN3 mRNA Interaction Randomizes and Diminishes the Amount of *CLN3* Transcript

The RNA-binding protein Whi3 emerged from a genetic screen for yeast cells that are small in size due to a premature passage through START, and the protein has been hypothesized to regulate the translation of *CLN3* transcripts (Nash et al., 2001; Wang et al., 2004; Garí et al., 2001). The *Ashbya CLN3* sequence contains multiple copies of the Whi3 binding consensus sequence

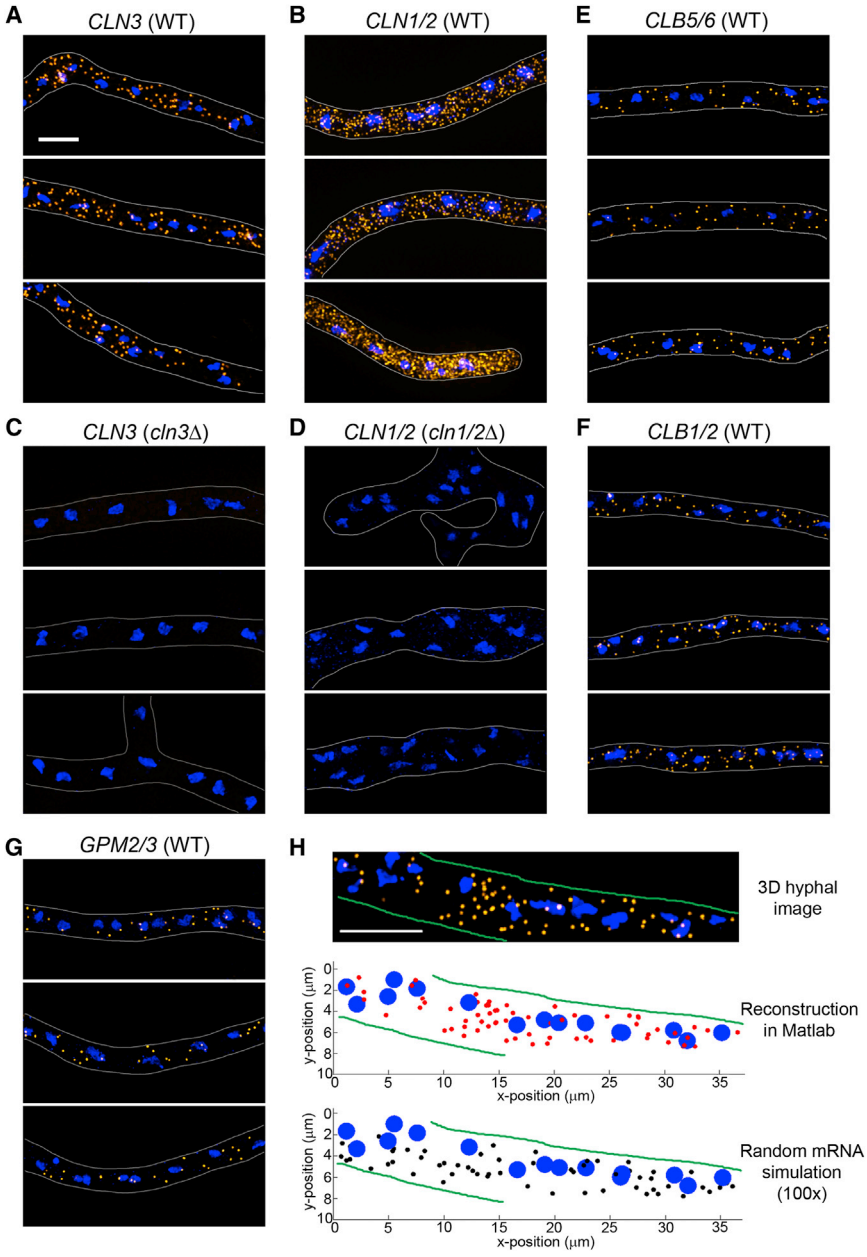

Figure 1. Cyclin Transcripts Are Variably Distributed in Cytoplasm in *Ashbya*

(A–G) Each cyclin transcript (orange) is visualized in wild-type *A. gossypii* or null mutant strain by single-molecule RNA FISH. Nuclei (blue) are visualized by Hoechst staining. Images are projected through the z axis. Cell boundary is in gray. Scale bar represents 5 μm.

(H) One example of RNA FISH image processing. Top: a 3D hyphal image is acquired and imported into ImageJ to automatically detect mRNAs (orange), nuclei (blue), and cytoplasmic area (green lines) in 3D. Middle: the information of detected spots such as x, y, z coordinates, volumes, and signal intensities are imported into MATLAB for further analyses. Bottom: spatially random mRNAs are simulated using Poisson distribution using the same mRNA density as the input data. One of 100 simulated random mRNA sets (black) is shown. Scale bar represents 5 μm. See also Figure S1.

(Figure S4A) and *Ashbya* Whi3 protein binds *CLN3* mRNA based on RNA immunoprecipitation (RIP) (Figure 3I). We then tested whether *CLN3* transcript localization patterns change when the *Ashbya* homolog of Whi3 was eliminated (Figure 3). In contrast to wild-type, *CLN3* transcript was spatially randomly distributed in *whi3*Δ mutants as indicated by the loss of the bimodal distribution of intertranscript distances (Figure 2B) and the spatially random clustering index in the Ripley's K test (Figures 3G and 3H). The randomization in the *CLN3* transcript localization depends upon the RNA-binding ability of Whi3, as C-terminal truncation mutants lacking the RRM have a similar RNA distribution pattern as the *whi3* null (Figures 2B, 3D, 3G, and 3H). This is not a consequence of perturbing the C terminus of the protein more generally because a truncation that retains the RRM but is deleted for the last 29 aa of Whi3 is also clustered (data not shown). Additionally, *CLN3* transcripts with silent point mutations in six predicted Whi3 binding sites (*cln3*-6 m) no longer bind to Whi3 in an in vitro protein-RNA binding assay (Figures 3F and 3J) and phenocopy the *whi3* mutants in terms of producing a spatially random *CLN3* mRNA localization (Figures 2A, 2B, 3G, and 3H). Both *whi3* mutants and the *cln3*-6 m also show a decreased number of transcripts per cytoplasmic area indicating that the association of *CLN3* mRNA with Whi3 is important both for clustering and stabilizing the transcript (Figures 3C, 3D, and 3F). These data show that Whi3 is required for the nonrandom clustering of *CLN3* mRNA in the cell.

Heterogeneous Localization of Whi3 Protein Requires a PolyQ Sequence

If Whi3 controls nonrandom spatial organization of *CLN3* transcripts, we predicted that the Whi3 protein is also distributed nonuniformly in the cytoplasm. Whi3-2XGFP was expressed as the only copy in the cell at the genomic locus under control of the native promoter. These cells grew normally, had no cell-cycle defects, and *CLN3* transcripts localized similarly to wild-type cells (Figures 2, 3, and 5). Whi3 protein has a highly heterogeneous localization and forms puncta and tubules in the cytosol (Figure 4A) that are generally distinct from the endoplasmic reticulum (ER) (Figure 4B) and in contrast to a homogeneous localization of soluble green fluorescent protein (GFP) (Figures 4E and 4F). We identified a stretch of glutamines (polyQ region) in the middle of the Whi3 primary sequence (73 Glutamines over a 150 amino acid length) and hypothesized that this polyQ stretch has the potential to

create aggregates or clusters of Whi3 protein (Figure S4). To evaluate the function of the polyQ region, we replaced the core polyQ sequence with six copies of an HA epitope tag. When this construct was expressed as the sole copy of Whi3 in cells, the localization became homogeneous and there were not detectable puncta or tubules however the protein was found at levels comparable to wild-type (Figures 4C, 4F, and 4G).

PolyQ stretches in the primary sequence are hallmarks of prions and other aggregation-prone proteins. We hypothesized that the polyQ sequence may be generating complexes of Whi3 that would be less freely diffusing than monomeric proteins. When the behavior of single molecules of Whi3-GFP was compared to GFP alone using fluorescence correlation spectroscopy (FCS), we found that substantially and significantly different autocorrelation curves and diffusion times were estimated, indicating that Whi3 behaves as a much larger complex (>50× slower than would be expected based on mass) than predicted based on its molecular weight (Figure 4H; see Supplemental Experimental Procedures for details of estimation). Similarly, the polyQ region of Whi3 when fused to GFP can induce soluble GFP to form puncta and slows the diffusion of GFP in the cytosol (Figures 4D, 4F, and 4H). We also have observed that Whi3 is significantly slower in diffusion than the Whi3ΔpolyQ protein (Figure 4I). Thus, endogenous Whi3 is localized into discrete puncta and tubules in the cytoplasm, and the polyQ region of the protein controls this heterogeneous localization.

Heterogeneous Whi3 Is Required for Transcript Clusters

PolyQ-mediated aggregation of Whi3 protein could be responsible for the clustering of *CLN3* mRNA. Indeed, when the polyQ region is missing from Whi3 and replaced with nonrepetitive neutral sequence, *CLN3* transcript spatial distribution is randomized and significantly less clustered than in wild-type cells (Figures 3E, G3, and 3H). Notably, in the *whi3*ΔpolyQ strain, *CLN3* mRNA density and Cln3 protein levels are comparable to wild-type (Figures S4C and S4D). This indicates that the Whi3ΔpolyQ protein is still functional in terms of *CLN3* regulation when the polyQ region has been replaced. Notably, in wild-type cells, we could also detect a small number of brighter single spots of *CLN3* transcript in the cytoplasm (indicated as tails in the distributions of intensity counts in Figure 2A and highlighted with asterisks in Figure 3), which are presumably subresolution clusters, and these high intensity spots are also diminished in the *whi3* mutants (Figures 2A; Kolmogorov-Smirnov (K-S) test of WT compared to *whi3*Δ, *whi3*ΔRRM, and *whi3*ΔpolyQ, $p < 0.01$). Importantly, although the polyQ-dependent aggregation behavior of Whi3 protein promotes clustering of *CLN3* transcript, Whi3 does not influence the localization or abundance of other cell-cycle transcripts (Figure S2).

We hypothesized that the clustering of transcripts leads to substantial nucleus-to-nucleus variability in local *CLN3* transcript abundance and this, in turn, could promote asynchronous nuclear division even within a common cytoplasm. To test this idea, we determined the position of *CLN3* mRNA clusters relative to the center of nuclei using our automated image analysis code and applied a bivariate form of the Ripley's K function that determines whether mRNA are nonrandomly positioned relative to nuclei. We found that the *CLN3* transcripts tend to be in the vicinity of nuclei rather than throughout the cell such that mRNA clusters are most common very close to the nuclear periphery (~0.75 μm, average nuclear radius is 0.5 μm) and at ~3 μm away from the center of each nucleus, which is near the peripheral zone of the neighboring nucleus (Figures 5A, S5C, and S5D). Interestingly, not all nuclei express *CLN3* (as indicated by bright foci of transcripts at a single spot within the nucleus that is presumably the gene), and in asynchronous cells only ~12% of nuclei appear transcriptionally active for this locus (Figure 5B). There is also variation in the proportion of nuclei expressing any of the different transcripts we analyzed, indicating that there are nuclear autonomous transcriptional programs running in these syncytial cells (Figure 5B). Nuclei that are actively expressing *CLN3* have on average similar transcripts in their vicinity as those that are not active and the transcripts are significantly clustered regardless of whether the nearest nucleus is transcriptionally active (Figures 5C and S4E). The positioning of transcripts in clusters near nuclei is associated with high variation in the number of transcripts per nucleus (Figures 5D and S5B). In *whi3* mutants, there is lowered nucleus-to-nucleus variability as indicated by a significantly smaller coefficient of variation in the distributions of transcripts per nucleus compared to the wild-type (Figures 5D and S5A).

We next evaluated whether adjacent nuclei that are neighbors in the same cell have widely varying numbers of transcripts. To address whether neighbors vary, the difference in transcript abundance was calculated for all pairs of adjacent nuclei and compared to differences that arise from a simulated random distribution for the same density of transcripts. We found that there was a significantly nonrandom distribution of differences between neighbors in the local abundance of *CLN3* (Figure 5E; $p < 0.03$, K-S test, differences between neighbors are greater than a random distribution for *CLN3*). Thus *CLN3* transcript clusters are found near nuclei, and transcript abundance varies substantially among nuclei in a single cell.

Nuclear Cycle Synchronizes when Cyclin Transcripts Are Randomized

We hypothesize that the clustering of transcripts generates a high degree of nucleus-to-nucleus variability in cell-cycle timing and promotes asynchrony of nuclear division in *Ashbya*. We next measured the level of nuclear cycle asynchrony in *whi3* mutants compared to wild-type cells and found that nuclei in *whi3* mutants became highly synchronous. Division synchrony was frequently captured in time-lapse movies in which three to four adjacent nuclei can be observed to divide simultaneously and in static measures of neighboring nuclei, in which many adjacent nuclei can be found in the same cell-cycle stage (Figures 6B and 6C; Movie S1; Table 1). Thus, homogeneous localization of *CLN3* is associated with increased nuclear synchrony. Additionally, division synchrony is observed when Whi3-*CLN3* mRNA interaction is abolished by the *cln3*-6 m mutant or when *WHI3* or *CLN3* is removed (Figure 6C). Importantly, the synchrony is not due to simply changing levels of *CLN3* transcript because the *whi3*ΔpolyQ strain shows comparable *CLN3* transcript and Cln3 protein abundance as wild-type but has synchronized cycle (Figures S4C and S4D). A further consequence of homogenization of the *CLN3* transcript is that the spacing between nuclei

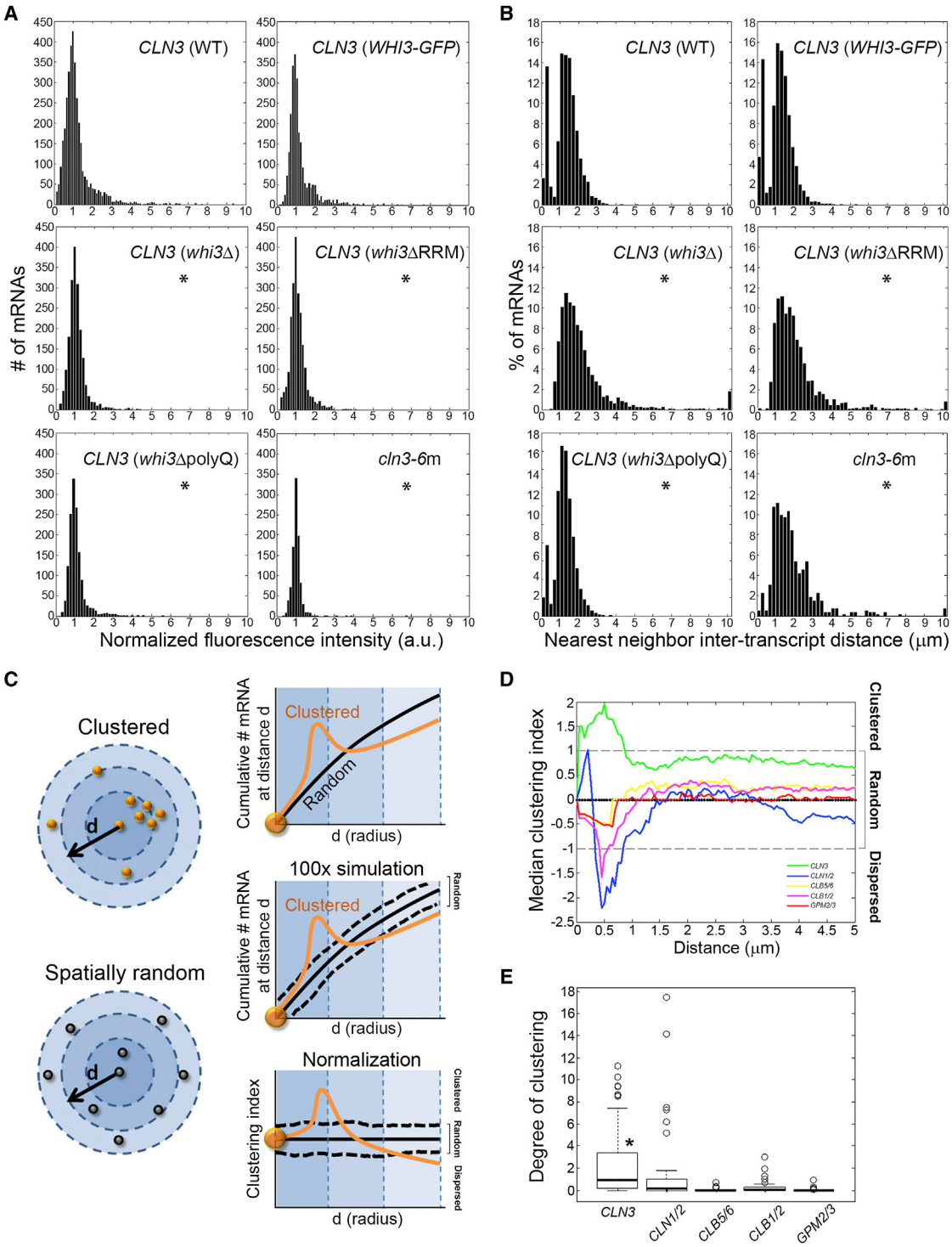

Figure 2. The G1 Cyclin *CLN3* Transcript Is Highly Clustered in the Cytoplasm

(A) Fluorescence intensity of *CLN3* transcript spots are normalized by mean signal intensity in each individual hyphal image for WT, *WHI3-GFP*, *whi3*Δ, *whi3*ΔRRM, *whi3*ΔpolyQ, and *cln3*-6 m (n = 3,130, 1,611, 2,435, 2,577, 3,826, and 1,071, respectively). The relative fluorescence intensities for all strains were compared to WT by the Kolmogorov-Smirnov (K-S) test with *p < 0.001.

(B) The nearest neighbor distances are measured for all *CLN3* transcript spots in each image and referred to as the intertranscript distances (ITDs). ITDs >10 μm are shown as 10 μm. ITDs in all strains were compared to WT by the K-S test with *p < 0.001. See also Figure S2.

(C) Spatial point pattern analysis using Ripley's K function. Left: a hypothetical case in which mRNAs are clustered (top) and another in which localization of mRNAs is spatially random (bottom). Top right: clustered mRNAs (orange) have distinctively higher cumulative number of mRNA at a particular distance (black). Middle right: black dotted lines are 95% confidence interval (CI) of a Poisson random mRNA distribution from 100 simulations. Empirical curve of

(legend continued on next page)

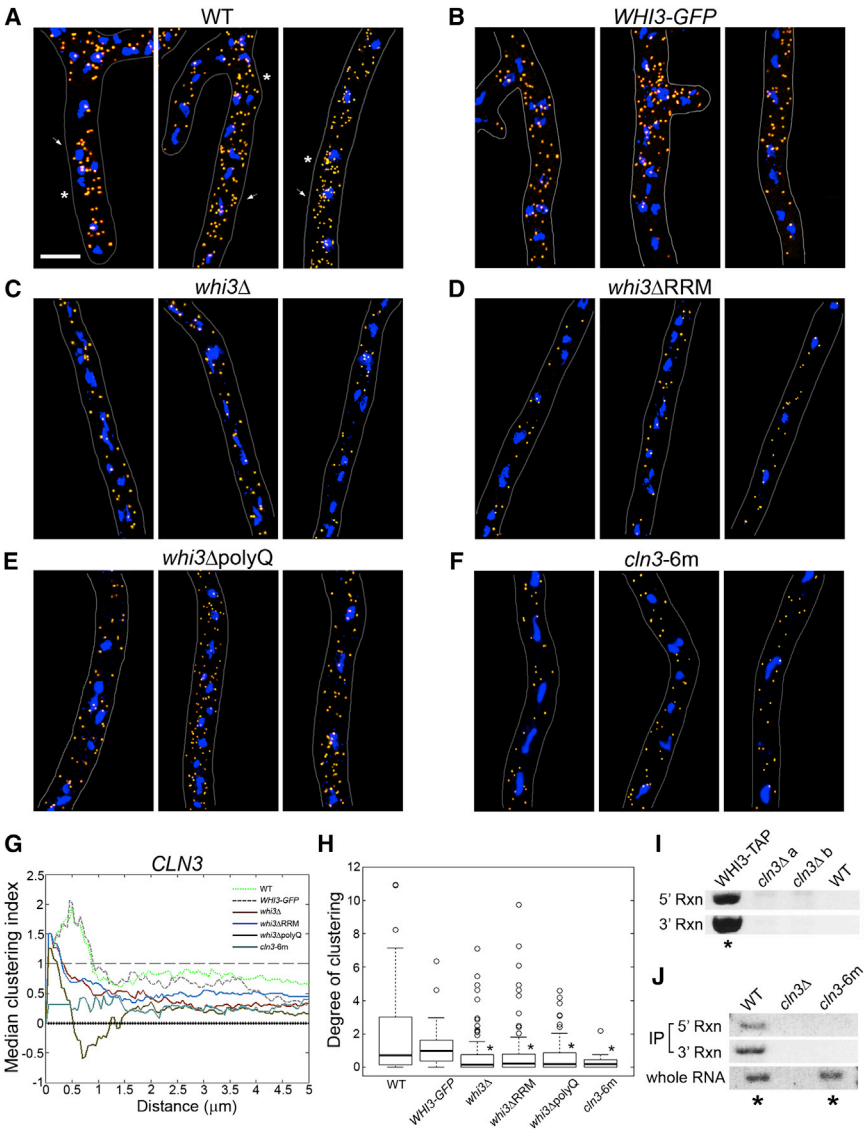

Figure 3. *CLN3* Transcript Clustering Requires the RNA-Binding Protein Whi3

(A–F) *CLN3* mRNA is visualized by single-molecule RNA FISH in WT, *whi3*, or *cln3*-6 m mutants. Cell boundary is in gray, mRNA is orange, nuclei are blue. (A) Arrow highlights large cluster, asterisk highlights subdifraction cluster. Scale bar represents 5 μm. See also Figure S4.

(G) Median clustering index (the median of Ripley's H(*d*)*) for *CLN3* mRNA in WT or *whi3* mutants; n > 72 for all strains. Light green, WT; dashed brown, *WHI3-GFP*; red, *whi3*Δ; blue, *whi3*ΔRRM; brown, *whi3*ΔpolyQ; blue, *cln3*-6m.

(H) Degree of clustering (the area of Ripley's H(*d*)* > 1). Degree of clustering for *CLN3* mRNA in *cln3*-6 m or *whi3* mutants are compared to WT. *p < 0.001 by Wilcoxon test. For the box-and-whiskers plot, bold line in the box: median, top, and bottom of the box: the third and first quartiles, respectively, whiskers: maximum and minimum of the data point excluding the outliers (open circle, data farther than 1.5× first or third quartile from the median).

(I) Whi3-mRNA complexes are pulled down using RNA immunoprecipitation (RIP) with magnetic beads (Dynabead, Invitrogen) conjugated with anti-Tap antibodies. cDNA are generated from purified mRNA and detected on the Southern blot and identified by sequencing (indicated *). Both 5′ and 3′ regions of *CLN3* ORF were amplified by PCR (5′ Rxn and 3′ Rxn).

(J) A direct interaction of Whi3 and *CLN3* mRNA is tested by in vitro binding assay (see In Vitro Protein-RNA Binding Assay). *CLN3* mRNA bound to Whi3 are detected on the Southern blot and identified (*). 5′ ORF of *CLN3* mRNA is amplified from whole mRNA to test if *CLN3* transcripts are expressed and sequenced (*).

See also Figure S3.

increases and also becomes more variable (Figure 6D; see also nuclei in Figures 3C–3E). This indicates that there is more cytoplasm per nucleus in *cln3*-6 m or *whi3* mutants and the number of nuclei per volume of cytoplasm is less constant when *CLN3* transcript position is randomized. This paradoxically suggests that the heterogeneous clustering of transcripts and, potentially, the timing asynchrony in general, ensures less fluctuation in nuclear-cytoplasmic ratios through time and space.

PolyQ Expansions Are Found in Many RRM-Containing Proteins

PolyQ and polyN domains have primarily been associated with pathological rather than physiological contexts in cells. However, linkage of a polyQ region that might influence protein oligomerization and diffusion to an RRM domain is a potential mechanism to generate spatially heterogeneous transcripts within a large cell or within a population of cells if such protein complexes are not symmetrically segregated at division. We therefore examined all of the RRM-containing proteins in *S. cerevisiae* and *Ashbya* for the presence of polyQ or polyN sequences and compared them to a set of

cumulative number of mRNA (orange) above 95% CI random range (black dashes) is indicative of clustering with p < 0.05. Bottom right: the cumulative number of mRNA is normalized by the upper random bound. See also Figure S3.

(D) Median clustering index is the median value of Ripley's H(*d*)* at distance d across all mRNA spots for each cyclin transcript (n > 55 cells for all transcripts). Green, *CLN3*; blue, *CLN1/2*; yellow, *CLB5/6*; magenta, *CLB1/2*; red, *GPM2/3*. See Figures S1 and S3 and Spatial Point Pattern Analysis for Single-Molecule RNA FISH Data.

(E) Area of plots of Ripley's H(*d*)* > 1 for each hyphal image is calculated for each cyclin transcript. This area is defined as "degree of clustering" where higher value indicates more clustering. Only degree of clustering for *CLN3* mRNA is significantly different from other transcripts. *p < 0.001 by Wilcoxon test. Kruskal-Wallis test is used for nonparametric ANOVA and Wilcoxon test is used for nonparametric multiple comparison test. For the box-and-whiskers plot, bold line in the box: median, top, and bottom of the box: the third and first quartiles, respectively, whiskers: maximum and minimum of the data point excluding the outliers (open circle, data farther than 1.5× the first or third quartile from the median).

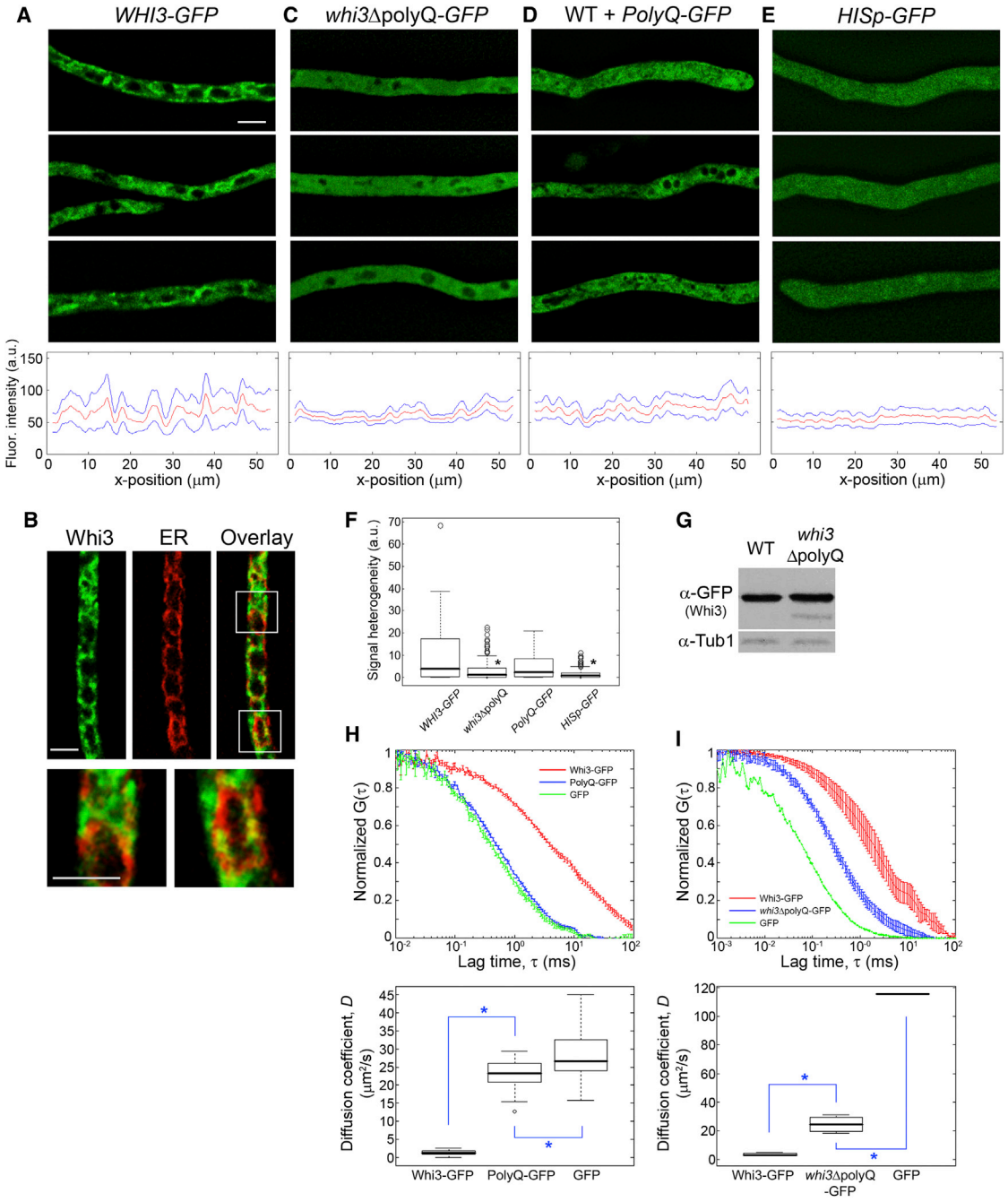

Figure 4. A PolyQ Expansion Is Required for Whi3 Heterogeneity and Can Limit Diffusivity

(A) Top: Whi3-2XGFP localization in live wild-type hyphae. Scale bar represents 5 μm. Bottom: fluorescence intensity from the top image is quantified below in the plot. Red line depicts the mean signal intensity along the hypha and range between two blue lines indicates the standard deviation of the signal intensity through the width of the hypha on each x position (see Signal Profile Plot for Assessment of Fluorescence Intensity Heterogeneity).

(B) Whi3 and ER (Sec63-mCherry) localization in the same cell. White boxes in overlay are magnified (6×) in bottom images. Scale bars represent 5 μm.

(C) Localization of Whi3ΔpolyQ-2XGFP in which PolyQ is replaced with 6HA epitope tags.

(D) PolyQ-GFP where the polyQ region of the *Ashbya* Whi3 is expressed in frame with GFP in addition to WT Whi3.

(E) Cytoplasmic soluble GFP is expressed in WT.

(F) Heterogeneity of mean fluorescence intensity along the hypha is quantified. The data are log10-transformed for ANOVA and multiple comparisons. n > 119 for all strains. *p < 0.001 by pairwise t test.

(G) *Ashbya* lysate pellet for the indicated strains grown at 30°C are separated on SDS-PAGE (10% acrylamide) and probed with anti-GFP or anti-Tubulin antibodies to quantify expression levels of Whi3. For α-GFP, an upper band is >260 kDa (dimer or higher) and a lower band is ~130 kDa (monomer).

(legend continued on next page)

proteins involved in glycolysis as a negative control. Remarkably, 50% of yeast RRM-containing proteins (n = 42 total protein sequences evaluated) and 26% of *Ashbya* RRM-containing proteins (n = 25) contained multiple runs of polyQs whereas no proteins involved in a control set of genes associated with glycolysis contained polyQ runs (n = 16 protein sequences evaluated). A recent bioinformatic analysis of RNA-binding proteins expressed in neurons found that 29 of 210 have substantial polyQ expansions predicted to produce aggregates (King et al., 2012). Thus, there are likely to be many different cellular processes that could exploit aggregation behavior of RNA binding proteins for normal physiological functions.

DISCUSSION

This study points to a mechanism to establish inhomogeneous distributions of RNAs and regulate the cell cycle through the employment of a polyQ region in an RNA-binding protein. We discovered that spatially nonrandom distribution of G1 cyclin transcripts is required for cell-cycle timing variability and asynchrony. Clustering of the cyclin transcripts requires a polyQ region in an RRM protein, Whi3. This polyQ expansion establishes a heterogeneous pool of Whi3 and likely serves to alter the diffusivity of Whi3 to create an uneven localization of transcripts in these large cells. We found many proteins containing RRMs also have polyQ repeats, indicating that this could be a general means for creating nonrandom distributions or gradients of RNAs within cells.

The pathological role of polyQ expansions has long been associated with prion-based and various neurodegenerative disorders. However, there has been only limited appreciation for a positive and regulatory role of protein aggregation in spatial patterning in cell biology. The CPEB protein, a regulator of translation, has been shown to more effectively function in an aggregated form in *Aplysia*, and the oligomeric state of CPEB is required for long term-memory formation in *Drosophila* (Majumdar et al., 2012; Si et al., 2003). In yeast, nucleoporins have been shown to have prion-like properties, although the functional role of this capacity outside of NPC assembly is not well understood (Halfmann et al., 2012b). Yeast has also been shown to use protein aggregation for epigenetic inheritance of traits for success in fluctuating environments (Halfmann et al., 2012a). There is also evidence of useful aggregation behavior in innate immunity responses to viral infections (Hou et al., 2011; Moresco et al., 2011), and functional amyloids are associated with storage of peptide hormones (Maji et al., 2009). These diverse but limited examples are likely only a glimpse of the actual physiological uses of unstructured and aggregation-prone proteins. A recent analysis of RRM-containing proteins enriched in the human brain found a surprisingly high frequency of polyQ regions (King et al., 2012). Our work provides evidence for a role of polyQ expansion in governing cyclin transcript position and regulating cell-cycle timing.

Cell-to-cell variation in cell-cycle timing is widely appreciated, although the sources of nongenetic phenotypic variation are not completely understood (Fantes and Nurse, 1977; Fox and Pardee, 1970; Gascoigne and Taylor, 2008; Hartwell and Unger, 1977; Koch and Schaechter, 1962; Lord and Wheals, 1980, 1981, 1983; Sennerstam and Strömberg, 1984; Spudich and Koshland, 1976; Tyson et al., 1979; Zetterberg and Larsson, 1985). Stochastic asymmetries in the segregation of aggregation prone RRM-containing proteins at mitosis could readily generate unequal cell behavior even between neighboring cells sharing a culture dish. Single-cell phenotypic variability would be exacerbated if there were various degrees of oligomerization of those proteins. The polyQs could generate different-sized oligomers with different diffusion capacity and ultimately lead to highly variable copy numbers between individual cells in a population. Additionally, clustering of transcripts via aggregation behavior of RNA-binding proteins could be a way to coordinate translation of transcripts in time and space or coordinate the translation of transcripts important for the same cellular process. Based on the appearance of steady-state fluorescence of Whi3-GFP and Whi3ΔpolyQ-GFP when expressed as the sole copy in the cell, it is clear that the polyQ region creates some nonuniform assemblies of Whi3 proteins in the cell. Supporting this, when Whi3-GFP is analyzed by FCS the diffusion time is >100 times slower than what would be expected based on its mass and shape (Slaughter et al., 2007) (Table S1). We speculate that polyQ expansions may be employed to tune the diffusivity of proteins and help to generate gradients or spatially inhomogeneous distributions of proteins or the processes they regulate.

Recent work has shown that RNA-binding proteins can self-assemble into gel-like assemblies in vitro due to the presence of highly unstructured regions in the polypeptides (Han et al., 2012; Kato et al., 2012). These assemblies are thought to mimic the formation of RNA-granules that are used for the packaging and directed transport of mRNAs to discrete locations, generally in polarized cells (Han et al., 2012; Kato et al., 2012). PolyQ/N sequences in P-body and stress granule components have also been shown to contribute to the assembly of very large MRNPs in yeast cells (Decker et al., 2007; Gilks et al., 2004). Based on our data, we envision that unstructured regions of RNA-binding proteins can also lead to the formation of smaller assemblies than an RNA granule that are important for spatially distributing the transcripts and potentially regulating stability and translation as well. Whether complexes of Whi3 proteins are homomeric or heteromeric and whether assembly and disassembly of the aggregates can be regulated are important questions for future investigation. Recently it has been suggested that the presence of polyN sequences, which are often also found in proteins with polyQs, can act in opposition to the polyQs and moderate the amyloid structures formed by pure polyQ runs (Halfmann et al., 2011) and Whi3 is also enriched in polyN sequences. We noticed a high frequency of histidines near the Whi3 polyQ region, raising the possibility that the aggregation could be regulated by metal binding.

(H and I) FCS measurements in live cells (G) or with bacterially expressed proteins (H). Top: autocorrelation curves for FCS. Bars represent standard errors (n > 10). FCS is performed with purified proteins for (H) due to the noise in live cells. Bottom: diffusion coefficients are calculated based on the fitting to a single component anomalous diffusion model. *p < 0.01 by Kruskal-Wallis test. For the box-and-whiskers plot, bold line in the box: median, top and bottom of the box: the third circle, data farther than 1.5× the first or third quartile from the median).
See also Figure S4.

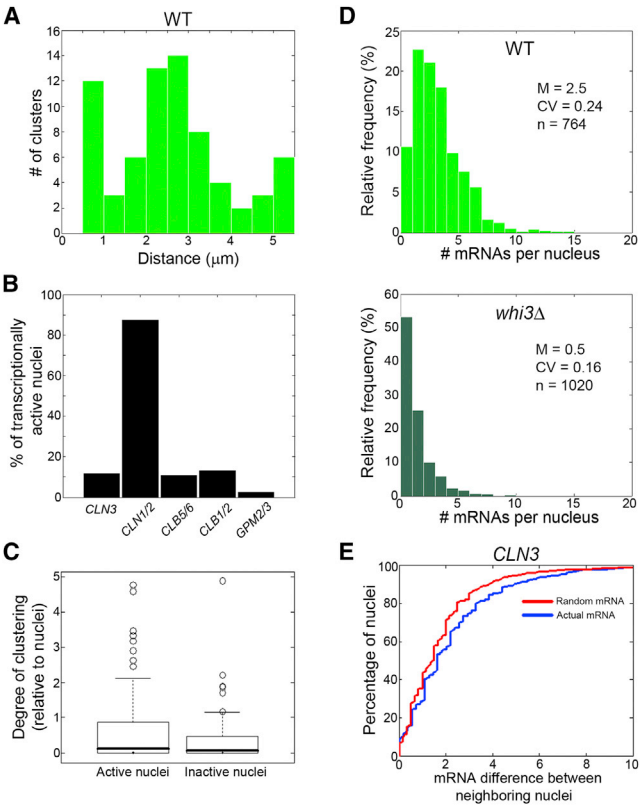

Figure 5. *CLN3* mRNA Clusters Are near Nuclei

(A) Histogram of distances of *CLN3* mRNA clusters from nuclei in WT. The histogram is binned by 0.5 μm and radius of a nucleus is ~0.5 μm.

(B) Percentage of nuclei that contain transcriptional hotspot (>1 mRNA in one mRNA spot within the nucleus) is obtained for all cyclin transcripts, n > 293.

(C) Degrees of clustering for transcriptionally active or inactive nuclei. An active nucleus contains a transcript spot with >1 *CLN3* mRNA. The difference between means are insignificant (p = 0.59 by Wilcoxon test). For the box-and-whiskers plot, bold line in the box: median, top, and bottom of the box: the third and first quartiles, respectively, whiskers: maximum and minimum of the data point excluding the outliers (open circle, data farther than 1.5× the first or third quartile from the median).

(D) Histogram of the number of mRNA within 2 μm radius centered on each nucleus in WT or *whi3* mutants, binned by 0.2 μm. Medians (M) and coefficient of variations (CV) are on the plots. See also Figure S5.

(E) Histogram of the difference between neighboring nuclei in the number of mRNA within a 2 μm radius (black bars) is compared the corresponding differences resulting from the simulation assuming CSR mRNA spots (red curve). p < 0.001 by K-S test. n > 630.

(F) Localization of Cln3-GFP in *Ashbya*. Nuclei are in blue. Red circle: nucleus based on DIC image. Cells are fixed and GFP-Booster (ChromoTek) was used to enhance the signal. Scale bar represents 5 μm.

Whi3 clearly plays a critical role in *Ashbya* in insulating nuclei so that the transcriptional products of the *CLN3* gene, a key G1 regulator, are not randomly distributed or presumably shared between adjacent nuclei. This provides a mechanism for insulating neighboring nuclei with regard to the early stages of cell-cycle commitment. Because microscopy-based assays for translation in live cells are limited, it is not yet possible to determine whether Whi3 is inhibiting or enhancing translation of *CLN3* transcripts. Preliminary analysis of proteins that associate with Whi3 indicate a substantial enrichment in proteins that function in translation (C.L., Nicholas S. Anderson, A.S.G., unpublished data). It is clear that Whi3 does seem to stabilize the transcript because *cln3*-6 m, *whi3*Δ, or *whi3*ΔRRM mutants have substantially less cytoplasmic *CLN3* transcript, whereas the polyQ mutant has comparable levels of transcripts, but randomly placed (Figure S5). Nuclei synchronized in all the different Whi3 mutants regardless of the *CLN3* transcript abundance indicating that it is likely the spatial distribution rather the Cln3 levels per se that contributes to the timing variability.

In summary, we have discovered a mechanism of creating heterogeneous transcript localization in a large cell that has the consequence of establishing variability in cell-cycle timing. The functional role of a polyQ expansion in altering diffusivity of an RNA-binding protein is a mechanism that may be widely exploited to create cell-to-cell variability in diverse processes.

EXPERIMENTAL PROCEDURES

Cell Culture and Preparation for Microscopy

For single-molecule RNA FISH, wild-type *A. gossypii* and *whi3*Δ29 cells were grown in 10 ml *Ashbya* full media (AFM) with a proper antibiotics, such as G418 (200 μg/ml), or ampicillin (100 μg/ml) in a 125 ml baffled glass flask, shaking at 30°C for ~16 hr. *whi3*Δ and *whi3*ΔRRM cells were grown at 22°C due to temperature sensitivity and for ~41 hr to obtain similar biomass to wild-type *A. gossypii* culture. *whi3*ΔpolyQ-*2XGFP* cells were grown at 30°C for ~21 hr to obtain similar biomass to wild-type *A. gossypii* culture. *whi3*Δ, *whi3*ΔRRM, and *whi3*ΔpolyQ-*2XGFP* cells had similar hyphal shape and diameter and rarely showed split-tip growth, which are indicatives of the fast cell growth phase. The *A. gossypii* culture was then transferred to a 15 ml conical tube (Sarstedt) for centrifugation and prepared for mRNA FISH as described in Single-Molecule RNA Fluorescence In Situ Hybridization.

For epifluorescence microscopy, *A. gossypii* cells were grown as described above and collected by centrifugation at 350 rpm for 1 min in a 15 ml conical tube. AFM was removed and cells were resuspended in 10 ml mixed media (25% filter-sterilized AFM and 75% 2× low fluorescence media) to reduce the autofluorescence of the medium, placed on a 25% filter-sterilized AFM/75% 2× low fluorescence media gel-pad containing 1% dextrose on the top of a slide, covered with a coverslip, and imaged. For time-lapse imaging, the slide with 2× low fluorescence media soaked tissues was loosely sealed with transparent plastic wrap to reduce evaporation. Imaging was performed at 30°C for wild-type *A. gossypii* and 22°C for *whi3* mutants. Microscopic images of cells were acquired as described in Wide-Field Fluorescence Microscopy Setup and Image Processing.

Wide-Field Fluorescence Microscopy Setup and Image Processing

An AxioImager-M1 upright light microscope (Carl Zeiss) equipped with the following Zeiss oil immersion objectives was used: EC Plan_Neofluar 40×/1.3 numerical aperture (NA), Plan-Apochromat 63×/1.4 NA, Plan-Neofluar 100×/1.3 NA, and α Plan-Fluar 100×/1.45 NA. Chroma filter set 41025 and Zeiss filter set 38HE were used for visualization of GFP. Chroma filter sets 41002B and 41043 were used for visualizing TAMRA and mCherry, respectively. Hoechst staining was visualized using a Zeiss filter set 49. An Exfo X-Cite 120 lamp was employed as the fluorescence light source. A Hamamatsu Orca-ER (C4742-80-12AG) CCD camera driven by Volocity 4 (Improvision-PerkinElmer) was used for acquisition of images. Z stacks of still and time-lapse images were acquired at different slice sizes (0.3–1.5 μm) and resulting images were processed by fast or iterative deconvolution (100–120 iterations) using calculated point spread functions in Volocity 4. All still images were linearly contrast enhanced in Volocity 4 and Photoshop CS5 (Adobe). All images were acquired through >10 μm along the z axis to ensure that the nuclei, SPBs, and mRNAs in the cell were imaged completely.

Single-Molecule RNA Fluorescence In Situ Hybridization

Single-molecule RNA FISH protocol from Stellaris protocols for *S. cerevisiae* (Biosearch Technologies) was modified for *A. gossypii* and used for

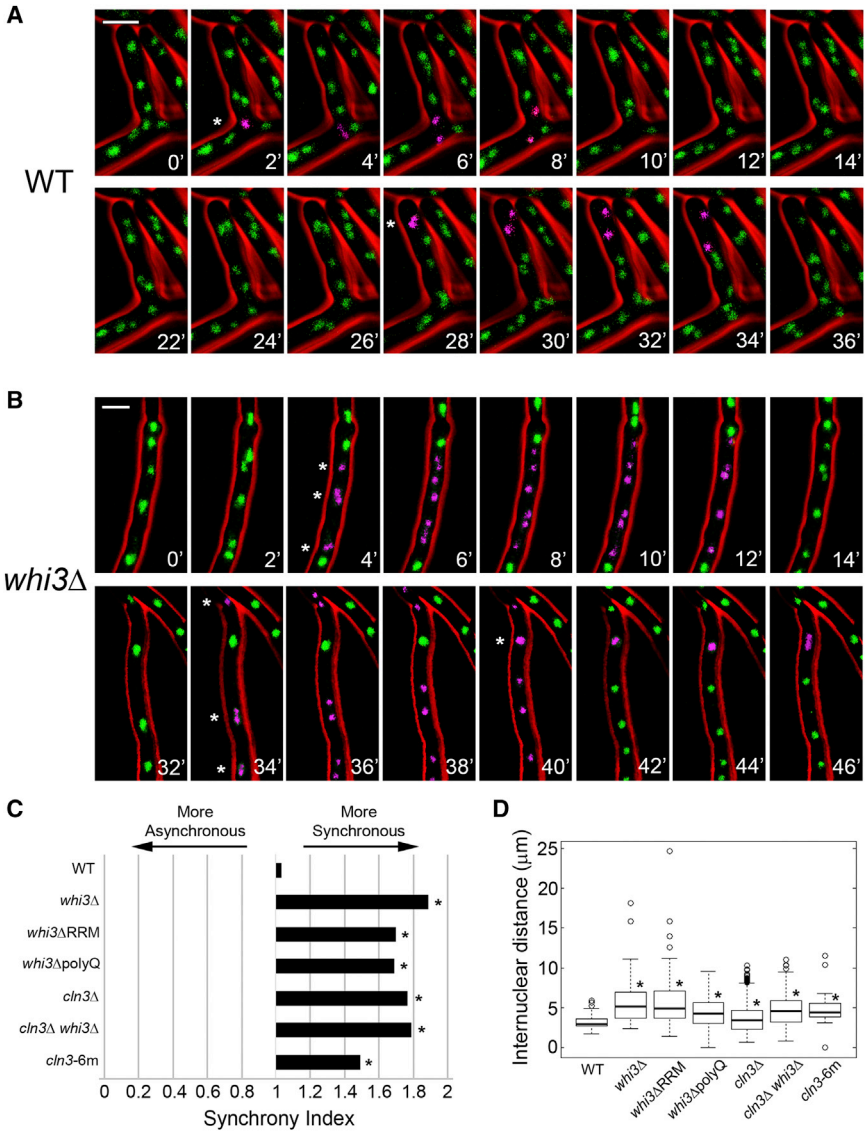

Figure 6. Nuclear Division Is More Synchronous in *whi3Δ* Than Wild-Type *Ashbya*

(A) Time-lapse of nuclear division in WT. Non-mitotic nuclei are in green, mitotic nuclei are in magenta and cell boundary is in red. Asterisk (*) indicates onset of mitosis. Scale bars represent 5 μm. See also Movie S1.

(B) Nuclear division in *whi3*Δ.

(C) The synchrony index for *whi3* mutants are compared to WT. *$p < 0.004$ by Wilcoxon test.

(D) Internuclear distances in *whi3* mutants are compared to WT ($n > 711$). *$p < 0.001$ by Wilcoxon test. For the box-and-whiskers plot, bold line in the box: median, top, and bottom of the box: the third and first quartiles, respectively, whiskers: maximum and minimum of the data point excluding the outliers (open circle, data farther than 1.5× the first or third quartile from the median).

visualization of mRNA. Cells were fixed in AFM with 3.7% v/v formaldehyde at 30°C for 1 hr on the shaker and washed twice with ice cold Buffer B (1.2 M sorbitol, 0.1 M potassium phosphate, pH 7.5). The cells were then resuspended in 1 ml spheroplasting buffer (10 ml buffer B, 2 mM vanadyl ribonucleoside complex) and transferred to a new RNase-free microcentrifuge tube. 1.5 mg Zymolase (MP Biomedicals) was added to the cells and incubated at 37°C for ~35 min for wild-type and ~10 min for *whi3Δ* cells, and they were washed twice with buffer B. Cells were resuspended in 1ml RNase-free 70% EtOH and incubated overnight at 4°C. RNA FISH probes from Stellaris were resuspended in 20 μl TE buffer (10 mM Tris Cl, 1 mM EDTA, pH 8.0). Then probes were diluted 1:10, 1:20, 1:50, or 1:100 from initial probe stock (250 μM in TE buffer) for optimal hybridization. On the next day, cells were washed with wash buffer (20× SSC, 10% v/v deionized formamide), resuspended in 100 μl hybridization buffer (1 g Dextran sulfate, 10 mg *E. Coli* tRNA, 2 mM vanadyl ribonucleoside complex, 2 mg BSA, 20× SSC, 10% v/v deionized formamide) with 2.5–250 nM mRNA FISH probe, and incubated in the dark, overnight at 37°C. On the third day, cells were washed with wash buffer, resuspended in wash buffer, incubated at 37°C for 30 min, washed again, and incubated in wash buffer with 5 μg/ml Hoechst (Invitrogen) for nuclear counterstaining at room temperature for 10 min. Cells were then washed with wash buffer, mounted on the RNase-free slide with 20 μl mounting media (ProLong Gold antifade reagent, Invitrogen), covered with an RNase-free coverslip, sealed with nail polish, and imaged.

Detection of Nuclei/mRNAs and Coordinate Reconstruction

The workflow of image processing and analysis is shown in Figure S1. Deconvolved z stack images were imported into ImageJ (Fiji 1.46a) and cropped so each image contains a single hypha. Customized C++ code was used for object detection in a fully automated and unbiased manner in ImageJ. Nuclei and mRNAs were detected separately with unique thresholds by the 3D-OC (3D object counter v2.0) plugin in ImageJ and cell boundary mask images were drawn from phase contrast images. x, y, and z coordinates of nuclei, mRNAs, cell boundary, and center of hypha including image information such as z step size and number of slices were then automatically exported from ImageJ and imported into MATLAB 2011b (MathWorks) for reconstructing hyphal images with nuclei, mRNAs, and cytoplasmic area in 3D in MATLAB. Hyphae were considered as curvy cylinders with changing radii. Size, volume, shape, and fluorescence signal intensity were considered to identify and calculate number of nuclei or mRNAs in a single spot. Thresholds for these criteria were set to remove background fluorescence, noise, or autofluorescent dirt. The threshold was calculated as 15% of mean mRNA/nucleus intensity in each image and objects with irregular shape were excluded from mRNA/nucleus detection. Using these calculations multiple mRNAs or nuclei in one spot were detected and counted based on the size and signal intensity compared to the mean values from all other spots in the working image. Multiple nuclei or mRNAs were generated within a single spot by slightly differentiating coordinates randomly using a Gaussian distribution. The mRNAs, nuclei, and cytoplasmic region reconstructed and recorded in MATLAB were used to calculate further metrics such as number of mRNA per nucleus or internuclear distance (IND). Statistical analysis of coordinate data involved running equal variance and normality tests to determine whether the assumptions of ANOVA and t tests were met. If at least one of them did not satisfy the requirements, the Kruskal-Wallis test (nonparametric version of ANOVA) or the Wilcoxon test (nonparametric version of the t test) were used for comparison. All processes were implemented and automated using customized MATLAB codes.

Table 1. Synchrony Index Summary

Genotype	Observed Synchrony (%)	Chance Synchrony (%)	SI	p Value[a]
WT	35.9	34.9	1.03	–
*whi3*Δ	62.2	32.9	1.89	<0.001
*whi3*ΔRRM	47.6	28.0	1.70	<0.004
*whi3*ΔpolyQ	57.5	34.1	1.69	<0.001
cln3Δ	53.8	31.9	1.76	<0.004
cln3Δ whi3Δ	54.5	30.4	1.79	<0.001
cln3-6 m	57.3	38.4	1.50	<0.004
*whi3*Δ29	39.3	33.3	1.18	>0.2

SI, synchrony index; WT, wild-type.
[a]Mutant versus WT, one-tailed t test.

Spatial Point Pattern Analysis for Single-Molecule RNA FISH Data

To quantitatively assess whether there is any structural pattern to the localization of cyclin transcripts within the cell, we used a method of spatial point pattern analysis called Ripley's K function (Ripley, 1981). Figure S3 depicts the following steps of our analysis for one sample image. In the present context, Ripley's K is defined as the ratio of the average number of mRNA points within a distance d of each mRNA to the overall mRNA density of the cell. Ripley's K, as a function of distance, can be estimated from data as

$$K(d) = n^{-2} V \sum_{i=1}^{n} \sum_{j \neq i}^{n} w(d)^{-1} I[D(i,j) \leq d],$$

where n is the number of mRNA spots, V is the total volume of the cytosol in which transcripts can locate, w is an edge correction function, I is a (0,1) indicator function, and D is the Euclidean distance.

Similarly, to quantitatively assess whether cyclin transcript clusters are found at a specific position relative to nuclei, we used the bivariate Ripley's K function (Ripley, 1981). In the present context, the bivariate Ripley's K is defined as the ratio of the average number of mRNA points within a distance d of the center of each nucleus to the overall mRNA density of the cell. Ripley's K, as a function of distance, can be estimated from data as

$$K_2(d) = (n_1 n_2)^{-1} V \sum_{i=1}^{n_1} \sum_{j \neq i}^{n_2} w(d)^{-1} I[D(i,j) \leq d],$$

where n_1 is the number of nuclei, n_2 is the number of mRNA spots, V is the total volume of the cytosol in which transcripts can locate, w is an edge correction function, I is a (0,1) indicator function, and D is the Euclidean distance.

To test the null hypothesis of complete spatial randomness (CSR), we simulated 100 random (Poisson-distributed) sets of mRNA locations for each observed cell, using overall mRNA density, cell geometry, and nuclear positions that matched those recorded for the cell. The use of identical geometry and nuclear positions preclude the need for an explicit edge correction in our calculation of K(d). The randomly generated sets of transcript positions were used to calculate 100 corresponding K-functions, and the mean and 95% outer limits of these functions were determined for each distance d. If the K(d) function for an actual, observed mRNA pattern extends above (or below) the outer bounds of the random distribution at any given distance d, then statistically significant clustering (or dispersion) at that distance can be concluded for that cell.

Under the CSR assumption and in the absence of edge effects, the expected value of K(d) equals $(4/3)\pi d^3$, the volume of a sphere of radius d. Therefore, to enhance graphical representation, we use the following transformation:

$$H(d) = \sqrt[3]{\frac{3K(d)}{4\pi}} - \sqrt[3]{\frac{3E[K_s(d)]}{4\pi}},$$

where $K_S(d)$ is Ripley's K function for the simulations representing CSR. Finally, by normalizing H(d) functions from each cell by the upper (or lower) bounds of the respective random simulations, we are able to show plots of all observed cells on a common scale. For visual clarity, we summarize the results across the many observed cells by plotting the median of these rescaled observed H(d) functions, or H(d)*. Where this line breaches the CSR 95% confidence envelope (bounded by ±1.0 after the rescaling), this indicates statistically significant clustering (or dispersion) across the many observed cells at that distance. The degree of clustering summarizes all the peak H(d) value for each image for a given transcript or genotype. Customized MATLAB code was used for all calculations and plots were generated in MATLAB 2010b or R v2.13.1.

Signal Profile Plot for Assessment of Fluorescence Intensity Heterogeneity

To assess whether localization of Whi3 vary along the length of hyphae, individual hyphal images with GFP fluorescence signal that were acquired and processed identically were imported and aligned with hyphae facing in the same direction in MATLAB. One slice in the middle of a z stacked image was used. Pixels in the field out of the cell or in the nucleus were eliminated by using a specific threshold to consider only fluorescence signal in the cytoplasmic area. Means and SDs of signal intensity were calculated in the direction of hyphal width on each pixel along the hypha and plotted on signal profile plots. A moving average over 10 pixels (1 μm) was applied to reduce small noise spikes on the plot. All local maximal or minimal peak points where mean signal intensity changed from positive to negative or vice versa were detected from the signal profile plots. The differences of signal intensity (a.u.) between two adjacent peak points were collected from each strain and the heterogeneity of signals from local peak points were compared on a box plot. The data were log-transformed for the statistical test. Customized MATLAB code was used for these processes.

Nucleus-to-Nucleus mRNA Heterogeneity Test

To determine whether neighboring nuclei have nonrandom differences in the local abundance of transcripts, spherical regions of interest (ROI) with radii of 2 μm was centered on each nucleus of the MATLAB reconstructed hypha and the number of mRNAs within each ROI was recorded. Similarly, the number of simulated random mRNAs in each ROI was also recorded. Next, the difference in number of mRNAs between two neighboring nuclei was calculated throughout the nuclei pairs within each hypha and recorded both for actual mRNAs and simulated random mRNAs in each strain for each transcript. K-S test was conducted on the recorded differences for actual mRNAs and simulated mRNAs to test if the heterogeneity in number of transcripts between neighboring nuclei with actual mRNAs was statistically significant compared to simulated random mRNAs. The p values and the differences in means (Delta) were recorded to estimate the significant heterogeneity in number of mRNAs on neighboring nuclei.

FCS Measurement and Analysis

Cells were incubated at 30°C for 15–16 hr in AFM media, centrifuged 1 min at 300 × g (Sorvail Legend Mach1.6R, Thermo Electron), and resuspended in 1 ml of 2× low fluorescence media, 15 μl of which was then added to the surface of a slide-thick agar gel pad (2% in 2× low fluorescence media). A coverslip (1.5 mm, Corning) was mounted and then VALAPed at the edges to prevent water loss as well as gel movement on the supporting slide.

To obtain bacterially expressed Whi3 proteins, *E. coli* containing AGB499 was incubated overnight at 37°C in 5 ml LB culture containing 2.5 μg Kanamycin. The culture was diluted at 1:60 to make a 50 ml LB culture containing 25 μg Kanamycin and incubated at 16°C for 3 hr. Then, IPTG (final concentration 1 mM) was added and the culture was incubated at 16°C for 30 hr. The bacterial culture was centrifuged at 3,000 × g for 15 min, resuspend the pellet in 630 μl lysis buffer (1% Tween-20, 10% glycerol, 300 mM NaCl, 50 mM NaH_2PO_2, 20 mM imidazole, 25× protease inhibitor cocktail, 70 μl 10 mg/ml lysozyme, and 7 μl 500 mM mercaptoethanol) and incubated on ice for 30 min. After sonication for 10 s, the sample was centrifuged at 13,200 rpm for 30 min at 4°C, the supernatant was loaded on the equilibrated Ni-NTA column (Qiagen) and centrifuged at 1,400 rpm for 5 min. Ni-NTA column was washed three times with 600 μl wash buffer (500 mM NaCl, 40 mM imidazole, 50 mM NaH_2PO_2) at 2,800 rpm for 2 min. The purified Whi3-2XGFP is eluted with 200 μl elution buffer (300 mM NaCl, 500 mM imidazole, 50 mM NaH_2PO_2).

Fluorescence lifetime correlation spectroscopy (FLCS) was carried out with a 485 nm pulsed laser at 20 MHz repetition frequency (PDL800-D, PicoQuant GmbH). The laser and the photon detecting unit are integrated to a laser scanning confocal microscope (Nikon A1). Pinhole was set to 1.0 Airy Unit. A 60×A/1.2 water immersion objective (Plan Apo VC, Nikon) was used, with the correction collar set to 1.75. A405/488 dichroic mirror was used as excitation filter and a 520/35 short-pass dichroic mirror was used as emission filter.

The autocorrelation function (ACF) obtained with afterpulsing suppression by means of FLCS in SymPhoTime (PicoQuant GmbH) was fitted directly to an anomalous diffusion model in SymPhoTime

$$G(\tau)=\frac{\gamma}{N}\left[1+\left(\frac{\tau}{\tau_D}\right)^{\alpha}\right]^{-1}\left[1+\frac{1}{\kappa^2}\left(\frac{\tau}{\tau_D}\right)^{\alpha}\right]^{-0.5}$$

(Gosch and Rigler, 2005; Schwille et al., 1999), where γ is a shape factor for the focal volume. For one photo excitation used here, $\gamma = 0.35$. N is the average number of molecules in the focal volume, τ_D is the diffusion time, α is the anomaly parameter, $\kappa = z_0/w_0$ is the length to diameter ratio of the focal volume by approximating the shape of the focal volume by a Gaussian profile, with z_0 as the effective focal radius along the optical axis at $1/e^2$ intensity and w_0 as the effective lateral focal radius at $1/e^2$ intensity. $V_{eff}=\pi^{3/2}w_0^2z_0$ is the effective excitation volume. The diffusion coefficient D is given by$D=w_0^2/(4\tau_D)$. Fitting results from FCS were exported to ASCII and imported to MATLAB (version 2011b, MathWorks) for plotting and statistical analysis.

The effective volume was calibrated by fitting the autocorrelation curve of 1.2 nM fluorescence dye ATTO488 in mini-Q water (ATTO-TEC GmbH) to a triplet-state model

$$G(\tau)=\left(1-T+Te^{-\frac{\tau}{\tau_t}}\right)\frac{\gamma}{N}\left(1+\frac{\tau}{\tau_D}\right)^{-1}\left(1+\frac{\tau}{\kappa^2\tau_D}\right)^{-0.5}$$

(Gosch and Rigler, 2005), where T is the (triplet) fraction of molecules, and τ_t is the lifetime of the triplet state. A length to diameter ratio of the focal volume $\kappa = 5.15 \pm 0.35$ was obtained from the fitting. With the known diffusion coefficient D of ATTO 488, the fitted τ_D from the autocorrelation curve, a confocal volume $V_{eff} = 0.25 \pm 0.05$ fl was obtained.

SUPPLEMENTAL INFORMATION

Supplemental Information includes Supplemental Experimental Procedures, five figures, one table, and one movie and can be found with this article online at http://dx.doi.org/10.1016/j.devcel.2013.05.007.

ACKNOWLEDGMENTS

We are grateful for valuable discussions from the Gladfelter Laboratory and thank Erik Grifin, Danny Lew, Rebecca Meseroll, Jamie Moseley, Samantha Roberts, and Roger Sloboda for commenting on the manuscript. We are grateful for Ann Lavanway's technical support for FCS. This work is supported by National Institutes of Health grant R01GM081506 and the Quantitative Biomedical Sciences program at Dartmouth College.

Received: September 7, 2012
Revised: January 28, 2013
Accepted: May 7, 2013
Published: June 13, 2013

REFERENCES

Berleth, T., Burri, M., Thoma, G., Bopp, D., Richstein, S., Frigerio, G., Noll, M., and Nüsslein-Volhard, C. (1988). The role of localization of bicoid RNA in organizing the anterior pattern of the Drosophila embryo. EMBO J. *7*, 1749–1756.

Cardoso, M.C., Leonhardt, H., and Nadal-Ginard, B. (1993). Reversal of terminal differentiation and control of DNA replication: cyclin A and Cdk2 specifically localize at subnuclear sites of DNA replication. Cell *74*, 979–992.

Decker, C.J., and Parker, R. (2012). P-bodies and stress granules: possible roles in the control of translation and mRNA degradation. Cold Spring Harb. Perspect. Biol. *4*, a012286.

Decker, C.J., Teixeira, D., and Parker, R. (2007). Edc3p and a glutamine/asparagine-rich domain of Lsm4p function in processing body assembly in Saccharomyces cerevisiae. J. Cell Biol. *179*, 437–449.

Dietrich, F.S., Voegeli, S., Brachat, S., Lerch, A., Gates, K., Steiner, S., Mohr, C., Pöhlmann, R., Luedi, P., Choi, S., et al. (2004). The Ashbya gossypii genome as a tool for mapping the ancient Saccharomyces cerevisiae genome. Science *304*, 304–307.

Fantes, P., and Nurse, P. (1977). Control of cell size at division in fission yeast by a growth-modulated size control over nuclear division. Exp. Cell Res. *107*, 377–386.

Fox, T.O., and Pardee, A.B. (1970). Animal cells: noncorrelation of length of G1 phase with size after mitosis. Science *167*, 80–82.

Garí, E., Volpe, T., Wang, H., Gallego, C., Futcher, B., and Aldea, M. (2001). Whi3 binds the mRNA of the G1 cyclin CLN3 to modulate cell fate in budding yeast. Genes Dev. *15*, 2803–2808.

Gascoigne, K.E., and Taylor, S.S. (2008). Cancer cells display profound intra- and interline variation following prolonged exposure to antimitotic drugs. Cancer Cell *14*, 111–122.

Gilks, N., Kedersha, N., Ayodele, M., Shen, L., Stoecklin, G., Dember, L.M., and Anderson, P. (2004). Stress granule assembly is mediated by prion-like aggregation of TIA-1. Mol. Biol. Cell *15*, 5383–5398.

Gladfelter, A.S. (2006). Nuclear anarchy: mitosis in multinucleated cells. Curr. Opin. Microbiol. *9*, 547–552.

Gladfelter, A.S., Hungerbuehler, A.K., and Philippsen, P. (2006). Asynchronous nuclear division cycles in multinucleated cells. J. Cell Biol. *172*, 347–362.

Gosch, M., and Rigler, R. (2005). Fluorescence correlation spectroscopy of molecular motions and kinetics. Adv. Drug Deliv. Rev. *57*, 169–190.

Halfmann, R., Alberti, S., Krishnan, R., Lyle, N., O'Donnell, C.W., King, O.D., Berger, B., Pappu, R.V., and Lindquist, S. (2011). Opposing effects of glutamine and asparagine govern prion formation by intrinsically disordered proteins. Mol. Cell *43*, 72–84.

Halfmann, R., Jarosz, D.F., Jones, S.K., Chang, A., Lancaster, A.K., and Lindquist, S. (2012a). Prions are a common mechanism for phenotypic inheritance in wild yeasts. Nature *482*, 363–368.

Halfmann, R., Wright, J.R., Alberti, S., Lindquist, S., and Rexach, M. (2012b). Prion formation by a yeast GLFG nucleoporin. Prion *6*, 391–399.

Han, T.W., Kato, M., Xie, S., Wu, L.C., Mirzaei, H., Pei, J., Chen, M., Xie, Y., Allen, J., Xiao, G., and McKnight, S.L. (2012). Cell-free formation of RNA granules: bound RNAs identify features and components of cellular assemblies. Cell *149*, 768–779.

Hartwell, L.H., and Unger, M.W. (1977). Unequal division in *Saccharomyces cerevisiae* and its implications for the control of cell division. J. Cell Biol. *75*, 422–435.

Hou, F., Sun, L., Zheng, H., Skaug, B., Jiang, Q.X., and Chen, Z.J. (2011). MAVS forms functional prion-like aggregates to activate and propagate antiviral innate immune response. Cell *146*, 448–461.

Johnson, R.T., and Rao, P.N. (1970). Mammalian cell fusion: induction of premature chromosome condensation in interphase nuclei. Nature *226*, 717–722.

Johnson, R.T., and Rao, P.N. (1971). Nucleo-cytoplasmic interactions in the achievement of nuclear synchrony in DNA synthesis and mitosis in multinucleate cells. Biol. Rev. Camb. Philos. Soc. *46*, 97–155.

Kato, M., Han, T.W., Xie, S., Shi, K., Du, X., Wu, L.C., Mirzaei, H., Goldsmith, E.J., Longgood, J., Pei, J., et al. (2012). Cell-free formation of RNA granules: low complexity sequence domains form dynamic fibers within hydrogels. Cell *149*, 753–767.

King, O.D., Gitler, A.D., and Shorter, J. (2012). The tip of the iceberg: RNA-binding proteins with prion-like domains in neurodegenerative disease. Brain Res. *1462*, 61–80.

Kiskowski, M.A., Hancock, J.F., and Kenworthy, A.K. (2009). On the use of Ripley's K-function and its derivatives to analyze domain size. Biophys. J. *97*, 1095–1103.

Koch, A.L., and Schaechter, M. (1962). A model for statistics of the cell division process. J. Gen. Microbiol. *29*, 435–454.

Lécuyer, E., Yoshida, H., Parthasarathy, N., Alm, C., Babak, T., Cerovina, T., Hughes, T.R., Tomancak, P., and Krause, H.M. (2007). Global analysis of mRNA localization reveals a prominent role in organizing cellular architecture and function. Cell *131*, 174–187.

Lécuyer, E., Yoshida, H., and Krause, H.M. (2009). Global implications of mRNA localization pathways in cellular organization. Curr. Opin. Cell Biol. *21*, 409–415.

Lord, P.G., and Wheals, A.E. (1980). Asymmetrical division of Saccharomyces cerevisiae. J. Bacteriol. *142*, 808–818.

Lord, P.G., and Wheals, A.E. (1981). Variability in individual cell cycles of Saccharomyces cerevisiae. J. Cell Sci. *50*, 361–376.

Lord, P.G., and Wheals, A.E. (1983). Rate of cell cycle initiation of yeast cells when cell size is not a rate-determining factor. J. Cell Sci. *59*, 183–201.

Maji, S.K., Perrin, M.H., Sawaya, M.R., Jessberger, S., Vadodaria, K., Rissman, R.A., Singru, P.S., Nilsson, K.P., Simon, R., Schubert, D., et al. (2009). Functional amyloids as natural storage of peptide hormones in pituitary secretory granules. Science *325*, 328–332.

Majumdar, A., Cesario, W.C., White-Grindley, E., Jiang, H., Ren, F., Khan, M.R., Li, L., Choi, E.M., Kannan, K., Guo, F., et al. (2012). Critical role of amyloid-like oligomers of Drosophila Orb2 in the persistence of memory. Cell *148*, 515–529.

Mavrakis, M., Rikhy, R., and Lippincott-Schwartz, J. (2009a). Cells within a cell: Insights into cellular architecture and polarization from the organization of the early fly embryo. Commun. Integr. Biol. *2*, 313–314.

Mavrakis, M., Rikhy, R., and Lippincott-Schwartz, J. (2009b). Plasma membrane polarity and compartmentalization are established before cellularization in the fly embryo. Dev. Cell *16*, 93–104.

Moresco, E.M., Vine, D.L., and Beutler, B. (2011). Prion-like behavior of MAVS in RIG-I signaling. Cell Res. *21*, 1643–1645.

Nair, D.R., D'Ausilio, C.A., Occhipinti, P., Borsuk, M.E., and Gladfelter, A.S. (2010). A conserved G_1 regulatory circuit promotes asynchronous behavior of nuclei sharing a common cytoplasm. Cell Cycle *9*, 3771–3779.

Nash, R.S., Volpe, T., and Futcher, B. (2001). Isolation and characterization of WHI3, a size-control gene of Saccharomyces cerevisiae. Genetics *157*, 1469–1480.

Ripley, B.D. (1977). Modelling spatial patterns. J. R. Stat. Soc. Series B Stat. Methodol. *39*, 172–192.

Ripley, B.D. (1981). Spatial Statistics (Hoboken, NJ: Wiley).

Schwille, P., Haupts, U., Maiti, S., and Webb, W.W. (1999). Molecular dynamics in living cells observed by fluorescence correlation spectroscopy with one- and two-photon excitation. Biophys. J. *77*, 2251–2265.

Sennerstam, R., and Strömberg, J.O. (1984). A comparative study of the cell cycles of nullipotent and multipotent embryonal carcinoma cell lines during exponential growth. Dev. Biol. *103*, 221–229.

Si, K., Lindquist, S., and Kandel, E.R. (2003). A neuronal isoform of the aplysia CPEB has prion-like properties. Cell *115*, 879–891.

Slaughter, B.D., Schwartz, J.W., and Li, R. (2007). Mapping dynamic protein interactions in MAP kinase signaling using live-cell fluorescence fluctuation spectroscopy and imaging. Proc. Natl. Acad. Sci. USA *104*, 20320–20325.

Spudich, J.L., and Koshland, D.E., Jr. (1976). Non-genetic individuality: chance in the single cell. Nature *262*, 467–471.

Takizawa, P.A., DeRisi, J.L., Wilhelm, J.E., and Vale, R.D. (2000). Plasma membrane compartmentalization in yeast by messenger RNA transport and a septin diffusion barrier. Science *290*, 341–344.

Tyson, C.B., Lord, P.G., and Wheals, A.E. (1979). Dependency of size of Saccharomyces cerevisiae cells on growth rate. J. Bacteriol. *138*, 92–98.

van den Bogaart, G., Meinema, A.C., Krasnikov, V., Veenhoff, L.M., and Poolman, B. (2009). Nuclear transport factor directs localization of protein synthesis during mitosis. Nat. Cell Biol. *11*, 350–356.

Wang, H., Garí, E., Vergés, E., Gallego, C., and Aldea, M. (2004). Recruitment of Cdc28 by Whi3 restricts nuclear accumulation of the G1 cyclin-Cdk complex to late G1. EMBO J. *23*, 180–190.

Weil, T.T., Forrest, K.M., and Gavis, E.R. (2006). Localization of bicoid mRNA in late oocytes is maintained by continual active transport. Dev. Cell *11*, 251–262.

Wu, C.W., Zeng, F., and Eberwine, J. (2007). mRNA transport to and translation in neuronal dendrites. Anal. Bioanal. Chem. *387*, 59–62.

Zenklusen, D., and Singer, R.H. (2010). Analyzing mRNA expression using single mRNA resolution fluorescent in situ hybridization. Methods Enzymol. *470*, 641–659.

Zetterberg, A., and Larsson, O. (1985). Kinetic analysis of regulatory events in G1 leading to proliferation or quiescence of Swiss 3T3 cells. Proc. Natl. Acad. Sci. USA *82*, 5365–5369.